



HAL
open science

A high resolution dose calculation engine for x-ray microbeams radiation therapy

Sarvenaz Keshmiri, Sylvan Brocard, Raphaël Serduc, Jean-françois Adam

► **To cite this version:**

Sarvenaz Keshmiri, Sylvan Brocard, Raphaël Serduc, Jean-françois Adam. A high resolution dose calculation engine for x-ray microbeams radiation therapy. *Medical Physics*, 2022, 49 (6), pp.3999-4017. 10.1002/mp.15637 . hal-03639046

HAL Id: hal-03639046

<https://hal.science/hal-03639046>

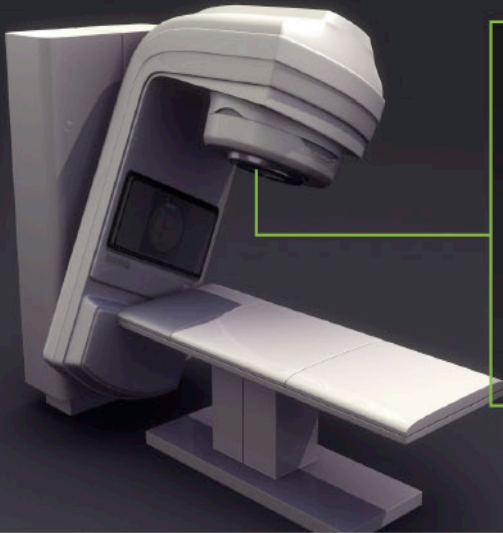
Submitted on 12 Apr 2022

HAL is a multi-disciplinary open access archive for the deposit and dissemination of scientific research documents, whether they are published or not. The documents may come from teaching and research institutions in France or abroad, or from public or private research centers.

L'archive ouverte pluridisciplinaire **HAL**, est destinée au dépôt et à la diffusion de documents scientifiques de niveau recherche, publiés ou non, émanant des établissements d'enseignement et de recherche français ou étrangers, des laboratoires publics ou privés.

RIT[®] TG142

THE SINGLE-VENDOR SOFTWARE SOLUTION FOR **EVERY QA TEST** RECOMMENDED IN TG-142



Perform comprehensive quality assurance of linear accelerators with confidence and ease, using an EPID and RIT software. Use either **RIT[®]TG142** or **RIT Complete** as your all-in-one software product for Machine QA, MLC QA, Imaging QA, and all the data tracking and trending you need to be in compliance with TG-142.



DAILY, MONTHLY, AND ANNUAL LINAC MACHINE QA TESTS



- Enhanced 3D Winston-Lutz (Isocenter Optimization)
- RIT's New Fully-Automated Star Shot Analysis
- Stereotactic Alignment (2D Winston-Lutz) Test
- Radiation/Light Field Coincidence
- Stereotactic Cone Profiles
- Field Alignment Test
- Electron Energy (TG-25)
- Asymmetric Field/Matchline
- Quick Flatness and Symmetry
- Water Tank Beam Measurement Analysis
- Depth Dose Profiles, Cross Profiles & Orthogonal Profiles

FAST AND EASY QUANTITATIVE MLC QA

- EPID Picket Fence Test
- Leaf Speed Tests for Varian and Elekta
- Hancock Tests for Elekta Machines
- Automated Varian RapidArc[®] Tests (0.1, 0.2, 0.2 HD, 1.1, 1.1HD, 1.2, 1.2 HD, 2 and 3)
- Bayouth MLC Test
- TG-50 Picket Fence Test
- MSK Leaf Test
- Varian DMLC Test Patterns
- MLC Transmission Analysis

ONE CLICK, INSTANT IMAGING QA

- Planar MV (EPID) Imager: EPID phantom, Las Vegas, PTW EPID QC, and Standard Imaging QC-3 Phantoms
- Planar kV Imaging: IBA Primus[®] L, PTW NORMI[®]-4, Leeds TOR-18 FG, and Standard Imaging QC-kv1 Phantoms
- CBCT/MVCT: CATPHAN[®] 504 and 604 for Varian, CATPHAN[®] 503 Elekta XVI and Siemens MVCT Phantoms
- Daily IGRT QA: ISOCube[™] Phantom kV-MV Isocenter Coincidence, CBCT Isocenter Coincidence, kV Collimation, MV Collimation/Light Field, and 6 Degree-of-Freedom Couch Tests

RIT software simplifies the process of creating a routine QA program at your facility, streamlines the reporting process for accreditation, and provides you with a better understanding of measurement performance across multiple machines and facilities.

SCHEDULE A PERSONAL DEMO OF RIT'S TG-142 CAPABILITIES TODAY!



RADIMAGE.COM[®]

+1.719.590.1077, Opt. 4 | sales@radimage.com | Connect with us on social media @RIT4QA  

©2022, Radiological Imaging Technology, Inc.

RapidArc[®] is a registered trademark of Varian Medical Systems, Inc.
CATPHAN[®] is a registered trademark of The Phantom Laboratory.

Primus[®] is a registered trademark of IBA.
ISOCube[™] is a trademark of IMT, Inc.
NORMI[®] is a registered trademark of PTW.



A high resolution dose calculation engine for x-ray microbeams radiation therapy

Running title: HR dose calculation in x-ray microbeams

Sarvenaz KESHMIRI¹, Sylvain BROCARD¹, Raphaël SERDUC^{1,2} and Jean-François ADAM^{1,2,*}

¹ Univ. Grenoble Alpes, INSERM, UA07 STROBE, 38000 Grenoble, France

² Centre Hospitalier Universitaire de Grenoble, 38000 Grenoble, France

*E-mail : jean-francois.adam@univ-grenoble-alpes.fr

Abstract

Background: Microbeam radiation therapy (MRT) is a treatment modality based on spatial fractionation of synchrotron generated x-rays into parallel, high dose, microbeams of a few microns width. MRT is still an under-development radiosurgery technique for which, promising preclinical results on brain tumors and epilepsy encourages its clinical transfer.

Purpose: A safe clinical transfer of MRT needs a specific treatment planning system (TPS) that provides accurate dose calculations in human patients, taking into account the MRT beams properties (high dose gradients, spatial fractionation, polarization effects). So far, the most advanced MRT treatment planning

This article has been accepted for publication and undergone full peer review but has not been through the copyediting, typesetting, pagination and proofreading process, which may lead to differences between this version and the [Version of Record](#). Please cite this article as [doi: 10.1002/mp.15637](https://doi.org/10.1002/mp.15637).

This article is protected by copyright. All rights reserved.

system, based on a hybrid dose calculation algorithm, is limited to a macroscopic rendering of the dose and does not account for the complex dose distribution inherent to MRT if delivered as conformal irradiations with multiple incidences. For overcoming these limitations, a multi-scale full Monte-Carlo calculation engine called penMRT has been developed and benchmarked against two general purpose Monte Carlo codes: penmain based on PENELOPE and Gate based on Geant4.

Methods: PenMRT, is based on the PENELOPE (2018) Monte Carlo (MC) code, modified to take into account the voxelized geometry of the patients (CT-scans) and offering an adaptive micrometric dose calculation grid independent to the CT size, location and orientation. The implementation of the dynamic memory allocation in penMRT, makes the simulations feasible within a huge number of dose scoring bins. The possibility of using a source replication approach to simulate arrays of microbeams, and the parallelization using OpenMPI have been added to penMRT in order to increase the calculation speed for clinical usages. This engine can be implemented in a TPS as a dose calculation core.

Results: The performance tests highlight the reliability of penMRT to be used for complex irradiation conditions in MRT. The benchmarking against a standard PENELOPE code did not show any significant difference for calculations in centimetric beams, for a single microbeam and for a microbeam array. The comparisons between penMRT and Gate as an independent MC code did not show any difference in the beam paths, whereas in valley regions, relative differences between the two codes rank from 1 to 7.5% which are probably due to the differences in physics lists that are used in these two codes. The reliability of the source replication approach has also been tested and validated with an underestimation of no more than 0.6% in low dose areas.

Conclusions: Good agreements (a relative difference between 0 to 8%) were found when comparing calculated peak to valley dose ratio (PVDR) values using penMRT, for irradiations with a full microbeam array, with calculated values in the literature. The high-resolution calculated dose maps obtained with penMRT are used to extract differential and cumulative dose-volume histograms (DVHs) and analyze treatment plans with much finer metrics regarding the irradiation complexity. To our knowledge, these are the first high-resolution

dose maps and associated DVHs ever obtained for cross-fired microbeams irradiation, which is bringing a significant added value to the field of treatment planning in spatially fractionated radiation therapy.

Keywords: Microbeam radiation therapy, dose calculation engine, Monte Carlo method, micrometric dose calculation grids, synchrotron radiation, medium energy x-rays.

1. Introduction

The outcome of radiation therapy in terms of efficacy and toxicity relies on a compromise made between maximizing the deposited radiation dose in the tumoral area and minimizing the damages to healthy tissues by keeping the radiation dose delivered to these organs as low as possible¹. Microbeam Radiation Therapy (MRT) is a disruptive radiotherapy approach aiming at widening the therapeutic window by combining the spatial fractionation of synchrotron generated x-rays into an array of intense parallel microbeams (25-50 μm wide beams replicated with a pitch of 200-400 μm) with an irradiation performed at high dose rate to benefit from the improved healthy tissue tolerance due to the FLASH effect²⁻⁴. MRT pushes the concept of dose volume effect to its theoretical limits with high doses delivered in the microbeam paths (peak doses), whereas low dose areas are found in-between these tracks (valley doses). Several preclinical studies have demonstrated the potential of MRT for improving tumour control with reduced side effects⁵⁻⁸.

The quality of MRT relies on several physical parameters, mainly the x-ray energy and the dose rate. The optimal energy for this treatment varies from 100 to 300 keV as shown by simulations⁹ and confirmed experimentally at the Australian Synchrotron¹⁰. Low to medium energy photons are required despite their lower penetration ability as they offer sharp penumbras and short lateral electronic equilibrium distances, thus keeping the dose between the microbeams as low as possible. Furthermore, the high dose rate is necessary to guarantee short irradiation times and minimize the blurring effect caused by the organ motions¹¹. The 3rd

generation synchrotron sources provide the high flux x-ray beams with the required spectral properties to be adequately used for MRT¹².

After two decades of preclinical studies, the clinical transfer of MRT in oncology and epilepsy management has started in the frame of large animal studies. Several challenging medical physics issues have to be managed to expand the concept of MRT to human patients treatments¹³. Accurate experimental dosimetry and online monitoring tools are being developed^{10,14}, together with state of the art dose calculation engines¹⁵, beam and patient positioning¹⁶ and patient specific quality assurance¹⁷.

In the past decade, numerous studies aimed at validating the dose calculation engines developed for microbeam radiotherapy. The majority of these calculation engines are based on Monte Carlo (MC) methods, considering the extremely small beam sizes and the properties of synchrotron x-rays. These studies were conducted using various MC codes, hence with different physical models: INHOM (EGS4)¹⁸, PENELOPE^{19–23}, Geant3 PSI-version²⁴, Geant4^{25–28}, EGS4^{29–31}, EGS5³², MCNPX³³ and EGSnrc³⁴. A comparative study by De Felici *et al.*, summarized the effect of different MC codes on in-field and out-of-field doses³⁴: in field doses were found similar amongst all the codes that have been investigated, whereas Geant4 gave significantly different out of field dose values.

The first attempt to create a MRT treatment planning system (TPS) being able to use an adequate dose calculation engine on dosimetry Computed Tomography (CT) data was performed by Martínez-Rovira *et al.*²², at the European Synchrotron Radiation Facility (ESRF) medical beamline (ID17). This full MC dose calculation algorithm based on PENELOPE/penEasy was modelling the whole ESRF medical beamline components. However, it could only be used for unidirectional treatment and non-conformal irradiation fields. The implementation of this method in a full TPS has been proposed, providing 3D conformal MRT could be performed in clinically compatible calculation times.

Several alternative methods aiming at drastically reducing the dose calculation time were proposed in order to reach a clinically compatible MRT TPS. A kernel based method was developed by Debus *et al.*³⁵. This remarkably fast algorithm is based on analytical pre-calculated kernels for scattered electrons and photons.

However, its accuracy is significantly lower at interfaces, valley areas and beam entrances and it is not able to take into account the photon polarization. Another simple but fast dose calculation algorithm with limited precision was developed by Poole *et al.*³⁶, based on pre-calculated peak to valley doses ratios (PVDRs) and ray-tracing. More recently, an hybrid algorithm has been developed by Donzelli *et al.*³⁷, at the ESRF-ID17. In this hybrid algorithm, the primary and scattered photons energy transfer is calculated using Geant4 MC code. Afterwards, the convolution of pre-calculated electrons dose kernels with the MRT fluence pattern creates peak doses. Valley doses are calculated from scattered photon interactions and added to the peak doses. According to the authors this method, is 600 times faster than a full straight forward Monte Carlo method. The cost of this rapidity is being limited to macroscopic rendering of separated peak and valley dose maps (see Fig 6 in Ocadiz *et al.*¹⁷). With the perspective of being used in MRT pre-clinical and clinical trials, some of these algorithms were successfully implemented in commercial TPSs. The kernel based method³⁵ has been coupled to VIRTUOS (A program for VIRTUal radiOtherapy Simulation and verification)¹⁵, the ray tracing method has been included in Eclipse TPS (Varian Medical Systems, Palo Alto, CA)³⁶ and recently, the hybrid algorithm is used as a calculation core for MRT in the research version of the Eclipse TPS³⁸. A summary of described existing algorithms is given in table 1.

Until now, none of the developed dosimetry tools combine all the requirements for a clinical use in a MRT dedicated TPS: precision, time efficiency and spatial resolution. In particular, as MRT leads to high dose gradients replicated at a micrometric scale inside the irradiation field, it is necessary to provide a precise micrometric dose calculation engine in order to understand the underlying radiobiological mechanisms of MRT, when being used as multi-directional treatments⁸.

In this study, we developed a full high-resolution MC dose calculation engine based on PENELOPE which is capable of taking into account the 3D conformal MRT fields, to be used as calculation core in a clinical MRT-

This article is protected by copyright. All rights reserved.

TPS. This calculation engine aims at being reliable, fast enough to ensure dose calculation in a clinical context. It should also allow the display of high resolution ($5\mu\text{m}$) dose maps and high resolution dose metrics for MRT.

Materials and Methods

Monte Carlo simulation code: PENELOPE

Since MRT deals with electron and photon energy lower than conventional radiotherapy in micrometric scale, the choice of an adequate Monte Carlo code has a crucial role. The choice of MC code depends on its simulation strategy class and implemented physical model. Among all the available MC codes, based on required characteristics, PENELOPE³⁹ was chosen for this work and upcoming developments. PENELOPE is a well-known MC code in the medical physics domain^{40,41} for simulating the photons and electrons/positrons transport within a wide energy range from 50 eV to 1 GeV in a large number of materials. The choice of PENELOPE is driven by the fact that PENELOPE uses a mixed simulation strategy, allowing detailed or condensed history calculations for the electrons/positrons transport, based on the compromises that should be made between the calculation time and the level of accuracy. Besides, its random-hinge algorithm provides a detailed description of low energy electron transport which is important for valley dose calculation. Compton differential cross-section (CDCS) is also a critical subject, as it can influence the absorbed dose in narrow passages of radiation (peaks), interfaces, entrance doses⁴² and the absorbed dose due to scattering (valley). In order to calculate CDCS, PENELOPE uses the Relativistic Impulse Approximation (RIA) rather than Klein-Nishina rough approximation or Waller-Hartree formalism³⁹. This approximation takes into account Doppler broadening and binding effects and it shows a good agreement with experimental data especially at low energies^{43,44}. Thanks to these features, PENELOPE has been used as a simulation tool for stereotactic radiosurgery⁴⁵ where a high precision is mandatory⁴⁶. Furthermore, the efficiency of this code in microdosimetry and nanodosimetry has been proven^{47,48}. Based on the aforementioned characteristics and also a precise model for polarized photons in PENELOPE (which is the case of synchrotron produced x-rays), this code can meet all specific requirements for MRT. In this work we developed a structured general-purpose

main Monte Carlo parallelized dose calculation engine for MRT, based on the latest version of PENELOPE (2018), but modified for accounting for MRT requirements.

PenMRT: PENELOPE for MRT

The main program developed for MRT is called penMRT (PENELOPE for MRT). The general-purpose main program (penmain) has been modified for being able to perform dose calculations in adaptive grids that are not linked to the CT scan voxel size, orientation and location. Penmain has also been modified to read voxelized geometries and quadric geometries at the same time. These modifications have been inspired by the work performed by Sempau *et al.* for penEasy⁴¹. A systematic parallelization using OpenMPI has also been implemented in penMRT. The comparison between block-diagrams of penmain and penMRT, shown on Figure 1, highlights the fundamental features of penMRT.

Geometric features of penMRT. PenMRT initializes the geometry and tracks particles in quadric geometries in the same ways as penmain (figure 1.a). However, if a voxelized geometry has been declared (based on a keyword “CT” in the initialization file), it activates the particle tracking specific to voxelized geometry (top box, figure 1.b). Thus, the voxelized geometry subroutine works alongside with quadric geometry subroutine to handle together voxelized structures and quadric structures in the same simulations without requiring temporary phase space files. The location tracking subroutine (LOCATE) has been modified so that if penMRT detects a particle entering a voxelized geometry, it calls its homologue in voxelized geometry subroutine (CTLOC, bottom box, figure 1.b).

In order to allow simulations for beams at various angles, it is required to rotate and translate each primary particle together with the dose calculation grid by using a specific subroutine (PCTSET). When the particles exit the CT structure, these modifications on trajectory and position are reversed by activating another subroutine (PCTUNSET). The advantage of this method is that, there is no longer a need for an external program to rotate the voxelized geometry such as in PenEasy or PenCT^{22,41,49}. Everything is now controlled in the main script,

which reduces the risk of potential errors. The subroutines responsible for determining the position and direction of particles after each event were kept intact. However, the JUMP subroutine is modified to provide a distance to travel in CT structure as well as in quadric geometry.

Radiation source replication in penMRT. In MRT, the radiation source consists of an array of microbeams separated by a desired center to center distance. This array is produced by using a so-called multislit collimator (MSC)⁵⁰. Planning in MRT also requires simulations of broad beams as the irradiation parameters are given in a reference non fractionated field. To that respect penMRT is able to account for both source geometries (Figure 2). The calculation time could be prohibitively long if the simulation includes the multislit because the amount of particles that are lost is higher than 85% of the primary particles generated from the source. Thus, to have an acceptable uncertainty in dose calculations, without increasing the calculation time, it has been decided to implement a source replication feature in penMRT (figure 2.b). To this respect a single microbeam source is modeled to the appropriate width and height. Each primary photon is then allocated to a given microbeam using a lateral translation ensuring random distribution in all the microbeams from the array. This feature is interesting because it can enable the modeling of non-homogeneous intensity profiles (roll off effect) by applying the distribution profile to the random translation.

Multi-scale adaptive dose grids in penMRT. Covering the whole patient data with a micrometric dose calculation grid demands a huge computational capacity and is not feasible in practice. Besides, a considerable fraction of the geometry receives a negligible dose. A function has been implemented in penMRT that establishes a multi-scale dose calculation grid and, with the possibility for the user to define the resolution of the dose calculation grids according to the area of interest. Typically, high resolution dose calculation grids are $0.005 \times 1 \times 1 \text{ mm}^3$, where the 0.005 mm is perpendicular to the incident beam axis in order to measure peaks, valleys and the transition of peak to valley zones. The medium and low resolution dose calculation grids are $1 \times 1 \times 1 \text{ mm}^3$ and $10 \times 10 \times 1 \text{ mm}^3$, respectively. It is desirable to cover the beam passage with a high resolution grid, and the user is free to choose the grid resolution and location, based on their specific needs. An example of dose calculation grids configurations is shown in Figure 3. With this adaptive dose calculation grid, penMRT is able to calculate dose maps at a micrometric and millimetric scale at the same time, to give a macroscopic vision of the entire zone irradiated by microbeam arrays.

PENELOPE simulations parameters for penMRT. In penMRT, the absorption energies (EABS), as well as the cut-off energies for hard inelastic events (WCC) and hard bremsstrahlung events (WCR) have been set to 10 keV for electrons and 1 keV for the photons³⁹. This ensures a mean free path of photons (2.51 μm in water at 1 keV) and a range of secondary electrons (2.45 μm in water at 10 keV) significantly smaller than the size of the dose calculation grids. Another important parameter which has an impact on charged particles transport is the maximum average angular deflection in multiple-scattering (C1) and the maximum average fractional energy loss along the step (C2) which are at the basis of the mixed approach of PENELOPE. The minimum value of C1 and C2 (C1=C2=0) results in a detailed time consuming simulation and on the contrary, the maximum values of C1 and C2 (C1=C2=0.2) accelerates simulations to the cost of a reduced precision in small dose grids^{39,46}. A detailed study was done by Martínez-Rovira *et al.*²² to quantify the effect of these parameters on calculation speed and the precision. In our study, three values of C1 and C2 values of 0.01, 0.05 and 0.1 were tested in order to find an optimal value for subsequent use. Synchrotron generated x-rays are linearly polarized in the horizontal plane²². As photon polarization affects the calculated dose away from the beam center²⁹, in performance tests, polarization is taken into account by setting the Stoke parameter P_3 to -1. Stoke parameter P_3 representing linear polarization and the value -1 meaning maximum polarization in horizontal plane.

Improved computational capacity and parallelization of penMRT. Originally, in PENELOPE, the memory allocation for dose calculation grids is a static allocation. This limits the computational capacity and the dose calculation is confined to a specific number of bins (typically 512 \times 512 \times 512). We implemented the dynamic allocation in penMRT instead of the static one, by using the Fortran 90 related features. The dose calculation capacity has been significantly increased with the dynamic allocation, allowing a continuous simulation of some hundreds of millions of dose bins and the production of simulation output files which is updated at the user specified time intervals; without memory issues. The memory capacity is a limiting factor. A typical simulation for a 2 \times 2 cm^2 MRT field with more than 10⁷ micrometric dose scoring bins needs 7 GB of memory per thread.

A “Single Program Multiple Data” (SPMD) scheme using OpenMPI⁵¹ has been implemented in penMRT, to be able to run the simulation on a cluster of CPUs, by using various sets of seeds in the random number generator used by PENELOPE, without recycling multiple times the results generated from the same seed and introducing unwanted bias.

Post-processing in penMRT

A set of post-processing scripts necessary for analyzing the results, has been developed for penMRT using Python 3.9 in order to visualize and analyze the dose maps. In case of multi-directional treatments, each beam is simulated separately (see figure 3.a and 3.b). The dose summation is performed using a custom made post processing script by rotating each dose map (figure 3.c) and resampling them into a $0.005 \times 0.005 \times 1 \text{ mm}^3$ dose bins (figure 3.d) and summing each incidence to create a unique high resolution dose map. Furthermore, another set of scripts dedicated to dose metrics and planning analysis, allow us to extract peak and valley dose maps separately based on the extraction method described by Ocadiz *et al.*¹⁷. Extracted peak and valley dose maps, could be used for dose prescription and absolute dose calculation and also comparisons with lower resolution peak and valley dose maps as obtained with the hybrid algorithm³⁷.

The same set of scripts allow us to go beyond the state of the art in dose metrics adapted to MRT. Typically in MRT peak (efficacy) and valley (toxicity) dose values have been studied as well as 1D dose metrics such as dose profiles or percentage depth dose (PDD) curves. The peak to valley dose ratio (PVDR) is also used as a quality indicator which qualifies the microbeam dose distribution with one number⁵². By using penMRT and high resolution dose maps, we were able to develop high resolution differential dose-volume histograms (dDVH) and cumulative dose-volume histograms (cDVH) in order to propose dose metrics that provide a clear rendering of the dose distribution complexity in MRT and tools for advanced treatment plan evaluation.

Cross-validations and performance tests on penMRT

Benchmarking of penMRT against penmain and Gate. As penMRT has been developed by modifying significantly a structured general purpose main program from PENELOPE, it must be first validated against the already benchmarked reference code penmain. In order to compare to an independent MC code, it has been

decided to use Gate (version 8.2)⁵³. Thus, a series of cross validation tests have been performed, based on dose maps, PDDs and dose profiles analysis, in order to validate penMRT. For comparison purposes, apart from the intrinsic differences in source geometry definition between Gate and PENELOPE and the chosen physics list, the same simulation parameters have been used in Gate than in penmain and penMRT. Indeed, in order to take into account the polarization effect, in Gate the “Livermore_polar” physics list has been used.

The spectrum which has been used by Martínez Rovira *et al.* in 2011²⁰ has been used for these cross-validations (average energy of 103.8 keV, see figure 2). As the goal of this work is to validate the reliability of penMRT, no variance reduction methods were used. Even if the beam divergence is negligible for synchrotrons x-rays; the small beam divergence has been taken into account in this study by positioning the radiation source 40.5 m away from the center of the phantom²⁰.

Performance tests on penMRT consists in comparing Gate, penmain and penMRT for various combinations of C1/C2 values:

- (i) For irradiations with a rectangular homogeneous $2 \times 2 \text{ cm}^2$ radiation field (broad beam): Penmain and Gate simulations were done in a quadric (figure 2.a) water phantom ($18 \times 18 \times 18 \text{ cm}^3$) and were manually parallelized on 10 CPUs. PenMRT simulations were carried out on a voxelized (figure 2.b) water phantom ($18 \times 18 \times 18 \text{ cm}^3$) with the parallelization performed using OpenMPI on 10 CPUs. To have an acceptable uncertainty, 10^{10} particles are simulated. Doses were scored in bins of $0.5 \times 1 \times 1 \text{ mm}^3$ and a zone of 180 (X direction) \times 180 (Y direction) \times 180 (Z direction) mm^3 centered at the center of the radiation field was covered by the dose grid. The calculation was done in about 1.2×10^7 voxels.
- (ii) For irradiations using a single microbeam ($50\mu\text{m} \times 2\text{cm}$ radiation field) in quadric and voxelized water phantom (figure 2): The simulation parameters and parallelization are the same as in (i). The comparisons were done on a single microbeam, because both penmain and Gate are neither capable of replicating the radiation source nor take into account the huge number of voxels which is necessary to cover the entire radiation field. Doses were scored in bins of $0.005 \times 1 \times 1 \text{ mm}^3$,

where the 0.005 mm dimension is perpendicular to the microbeam axis. A zone of 0.8 (X direction) \times 180 (Y direction) \times 30 (Z direction) mm³ centered at the center of the irradiation field was covered by the dose calculation grid. The calculation was done in about 1.3×10^6 voxels.

The results obtained by penmain, Gate and penMRT are compared by using the relative difference given by:

$$\delta = \frac{D_{penMRT} - D_{ref}(penmain/Gate)}{D_{ref}(penmain/Gate)} \quad (1)$$

In which, D is the calculated dose in each dose bin, with the reference values being set to the penmain and Gate results.

The 2D dose maps evaluation was carried out by the gamma index test, which is a pass-fail test using an ellipsoid of acceptance. The test is defined as follows⁵⁴:

$$\Gamma(r, D) = \sqrt{\frac{\Delta r^2}{\Delta d_M^2} + \frac{\Delta D^2}{\Delta D_M^2}} \leq 1 \quad (2)$$

Where ΔD_M and Δd_M are the acceptance criteria for the dose difference and the distance to agreement (DTA), respectively. If $\Gamma(r, D)$ stands between 0 and 1, the test passes, otherwise it fails. In our study, the dose map calculated by penmain (C1=C2=0.1) is taken as reference.

Performance tests of penMRT. Four distinct performances tests have been performed to study the capacities of penMRT for:

- (i) Dose profiles and depth doses curves for the study of monodirectional irradiations:

The abovementioned x-ray spectrum has been used (average energy of 103.8 keV). The simulations were performed using a conservative C1 and C2 value of 0.05. The source is an array of 51 microbeams (50 micrometer wide, 2 cm high), covering a 2×2 cm² field (400 micrometers spacing, center to center). A zone of 3 (X-direction) \times 18 (Y-direction) \times 3 (Z-direction) cm³ is covered with a high resolution dose grid, where X is the horizontal direction perpendicular to the

incident beam, Z is the vertical direction and Y is the beam propagation direction. This ensures a high resolution coverage of the whole beam path. The doses were scored in bins of 0.005 (X-direction) \times 1 (Y-direction) \times 1 (Z-direction) mm^3 . 2×10^9 primary particles have been simulated on 80 CPUs. In this case, calculation was done in 3.367×10^7 micrometric bins, more than 7.5×10^5 millimetric bins, and around 1300 centimetric bins, to cover all areas of interest in the simulation universe (water phantom and air around the phantom). The dose maps given by penMRT have also been benchmarked with penmain and Gate. As the simulation of an array of microbeam in the same condition as penMRT was not possible, a single microbeam was simulated in penmain and Gate. The absorbed doses were scored on a zone of 5 (X-direction) \times 6 (Y-direction) \times 3 (Z-direction) cm^3 in the pixels of 0.005 (X-direction) \times 1 (Y-direction) \times 1 (Z-direction) mm^3 . The obtained dose map was replicated 51 times with a pitch of $400 \mu\text{m}$ and summed to simulate the $2 \times 2 \text{ cm}^2$ field.

(ii) Source replication approach validation:

In order to validate the source replication strategy against a full modeling of the multislit collimator, a simulation of the irradiation geometry has been performed with the multislit collimator based on Martínez-Rovira *et al.*²⁰ calculations and compared to the source replication method in penMRT. The point source has been set at 40.5 m from the sample. The multislit collimator is defined according to Bräuer-Krisch *et al.*⁵⁰ and placed 1 m behind the sample. The simulations were performed using a harder spectrum, which is currently used for preclinical tests at the ESRF-ID17^{20,55} on large animals (121.7 keV average energy) to be in the worst transmission situation. The following parameters are used $C1/C2=0.05$, absorption energies of 10 keV and 1 keV for photons and electrons, respectively. The dose calculation grid resolution is set to $0.005 \times 1 \times 1 \text{ mm}^3$. A $410 \mu\text{m}$ center to center pitch for the source replication has been used for this comparison to account for the beam divergence in the simulation with a point source and collimator in place.

(iii) Cross-fired irradiation validation:

For benchmarking penMRT against penmain in cross-fired irradiation geometries. A single microbeam of $50 \mu\text{m} \times 2 \text{ cm}$ in a water phantom of $18 \times 18 \times 18 \text{ cm}^3$ is simulated with the same spectrum as (ii) and the doses are scored using the grids of $0.005 \times 1 \times 1 \text{ mm}^3$ on a zone of $5 \times 6 \times 3 \text{ cm}^3$. This dose map is then replicated with a pitch of $400 \mu\text{m}$ to simulate the $2 \times 2 \text{ cm}^2$ field. For each incidence angle, the dose maps are resampled (using `griddata` from the `scipy` package) to obtain $0.005 \times 0.005 \times 1 \text{ mm}^3$ dose bins and summed for each incidence. The same process of resampling and summation has been performed on penMRT dose maps. A $1 \times 1 \times 0.1 \text{ cm}^3$ region of interest (ROI) is chosen at the center of the dose maps for statistical comparison purposes. The similarity of dose distributions is investigated using a statistical Q-Q test (quantile-quantile plot) on the differential dose-volume histograms that are calculated on the ROI. The comparisons have been performed for the cross-fired irradiation protocol with two beams at 90° degrees.

(iv) Cross-fired irradiations using several microbeam arrays:

The simulations were performed using the same spectrum as (ii) and C1 and C2 were kept to a conservative value of 0.05. A dose calculation grid configuration is chosen in order to study the cross-firing region with a high resolution (figure 3.a). A zone of 3 (X-direction) \times 6 (Y-direction) \times 3 (Z-direction) cm^3 at the center of an $18 \times 18 \times 18 \text{ cm}^3$ water phantom was covered with the high resolution dose calculation grid of 0.005 (X-direction) \times 1 (Y-direction) \times 1 (Z-direction) mm^3 , where X is the horizontal axis perpendicular to the incident beam. The remaining of the geometry was covered by a $1 \times 1 \times 1 \text{ mm}^3$ dose calculation grid. The phantom was irradiated with a single (at 0°) and three (at 0° , 35° and 90°) irradiation beams. This performance test highlights the multiscale capabilities of penMRT as well as its capacity to simulate multi-directional treatments. The different beam incidences were simulated separately using 2×10^9 particles on 80 CPUs within more than 1.1×10^7 micrometric bins, 6×10^6 millimetric bins and 1300 centimetric bins.

The summed dose maps are thus obtained and displayed in $0.005 \times 0.005 \times 1 \text{ mm}^3$ voxels in abovementioned high resolution region, after rotation of each individual dose map. High resolution

differential dose-volume histograms (dDVH) are extracted on a $1 \times 1 \times 1 \text{ cm}^3$ region of interest centered on the treatment isocenter at the center of the phantom.

Results

PenMRT vs Penmain and Gate cross validation tests

Broad beam irradiation fields. For both, penMRT and penmain, simulation times of around 120, 50 and 36 hours were recorded on the ESRF cluster⁵⁶ to simulate 10^{10} primary showers, for C1 and C2 values of 0.01, 0.05 and 0.1, respectively (by doubling the C1 and C2 parameters, the simulation time decreases by a factor of 3.5). In the case of Gate, the simulation time was about 72 hours.

Isodose maps, gamma index maps and dose profiles calculated by penmain, Gate and penMRT in a phantom irradiated by a broad beam of $2 \times 2 \text{ cm}^2$ are compared at a depth of 2 cm in water on figure 4. The doses obtained with penmain using C1 and C2 values of 0.01 are taken as a conservative reference value compared to C1,C2 equal to 0.05 and 0.1 as suggested by Salvat *et al.*³⁹ and Martínez Rovira *et al.*²², respectively.

The 2D evaluation (2%, 1mm relative gamma index test, figure 4.a) shows a gamma index passing rate of 99% within the isodose 20%. The vertical deformation of the 5% isodose in figure 4.a highlights that the polarization effect has been properly taken into account. In figure 4.b and figure 4.d, the comparison of horizontal and vertical dose profiles between penmain, Gate and penMRT are showing an excellent agreement regardless of the C1 and C2 values. The comparison between the vertical and horizontal dose profiles shows the polarization effects on field edges and out-of-field doses. A maximum polarization of synchrotron generated x-rays in horizontal direction, causes a diminution of the out-of-field dose in the horizontal plane and an increase in the vertical plane. The polarization effect leads to similar results for penmain, Gate and penMRT (figure 4.d). The relative differences are plotted only for C1 and C2 equal to 0.01,0.1 and Gate, for not overcharging figure 4.c and 4.e. Figures 4.c and 4.e show that the relative difference is less than $\pm 0.5\%$ inside the irradiation field. The relative differences outside the irradiation field, beyond the 10% isodose, are higher and can reach a maximum of about $\pm 10\%$, due to the significant increase of the intrinsic statistical uncertainties. A two sigma uncertainty

level of 0.9%, 0.9% and 2.3% have been achieved in the beam center, penumbra and out-of-field (1.5 cm from the beam center), respectively.

The experimental doses as measured with a pinpoint ionization chamber agree with the doses calculated with penMRT and relative differences between 0.15 to 1.5 % are measured for depths ranging from 2 to 10 cm in solid water.

Single microbeam irradiation fields. For cross-validation of penMRT versus penmain and Gate in micrometric scale, simulation times of around 38, 19 and 8 hours were recorded on the ESRF cluster, to simulate 10^{10} primary showers, for C1 and C2 values of 0.01, 0.05 and 0.1, respectively. In the case of Gate the simulation time was about 48 hours.

Isodose maps, gamma index maps and dose profiles calculated by penmain, Gate and penMRT in a phantom irradiated by a single microbeam of $50 \mu\text{m} \times 2 \text{ cm}$ are compared at a depth of 2 cm in water on figure 5. The values obtained with penmain using C1 and C2 values of 0.01 are chosen as a conservative reference. A 100% passing rate for a relative gamma index test of $2\%/5\mu\text{m}$ is obtained (figure 5a). The relative difference on the doses calculated by penmain, and penMRT stays lower than 0.1% in the microbeam, and stays below 1% until the 5% isodose (figure 5.c) due to the statistical uncertainty increase. A two sigma uncertainty level of 0.2%, 0.3% and 4.8% has been achieved in the microbeam center, penumbra (the distance between 80% to 20% of the peak dose) and out-of-field (175 μm from the microbeam center), respectively.

Gate and penMRT comparison. Comparisons between Gate and penMRT show good agreement inside the irradiation field (differences lower than 0.1 %). This accordance decreases at the field edges which can be explained by the different strategies in source definition in these two separate simulations and by the use of different physical models. The differences in the physics lists can introduce discrepancies between the two simulations (around 10-15% for the broad beam, and around 5% for the single microbeam). These out of field or valley doses are mainly due to scattered photons and electrons transport. This difference in out-of-field doses calculated by PENELOPE and Livermore is also reported in other studies⁵⁷.

Percentage depth doses in broad beam and single microbeam fields. The PDD simulated for broad beams and one microbeam, using penmain, Gate and penMRT at various values of C1 and C2 are represented on figure 6. A good agreement between penmain and penMRT is observed for broad beam PDDs (figure 6.a and 6.b), with a maximum relative difference of $\pm 1.5\%$ in depth below 12.5 cm (which corresponds to the isodose 20%) and showing an increase of the statistical uncertainty coherent with the depth increase. An excellent agreement is observed between penmain and penMRT for a single microbeam. A maximum relative difference of less than $\pm 1\%$ is observed, independently of the considered depth (Figure 6.c and 6.d), because in that case, the 10^{10} particles are concentrated in the microbeam. As it is shown in figures 6.b and 6.d a relative difference lower than 1% is observed between penmain, Gate and penMRT. The discrepancies increases with depth to reach 6% and it might be due to the differences in the physical models in these two approaches.

PenMRT performance characterization

Full MRT field simulation. After benchmarking penMRT against penmain for broad beam and single microbeam simulations, the performance of penMRT was tested in full irradiation field of $2 \times 2 \text{ cm}^2$ consisting of an array of 51 microbeams (50 microns by 20 mm equally spaced, 400 microns center to center). In this case, a simulation time of 28 hours was recorded on the ESRF cluster (2×10^9 primary particles, dose calculation grid of $0.005 \times 1 \times 1 \text{ mm}^3$). A two sigma uncertainty level of 1.1%, 3% and 6% has been achieved in the beam center, penumbra and valley area (average on $100 \mu\text{m}$ centered at the valley center), respectively.

The dose map at 2 cm of depth, the horizontal dose profile in the center of the field, as well as the peak and valley PDDs are represented on figure 7. The PDD values (figure 7.c and 7.d) correspond to doses averaged on $0.01 \times 1 \times 1 \text{ mm}^3$ bins for the peak PDD, $0.1 \times 1 \times 1 \text{ mm}^3$ for the valley PDD. The peak dose PDD is varying as a decreasing mono-exponential function with depth. $\text{PDD}(y)=100\exp(-0.16084y)$, so the calculated linear attenuation coefficient is 0.1608 cm^{-1} , when the linear attenuation coefficient of water at 103.8 keV is 0.1687 cm^{-1} , which is less than 5% difference, using the monochromatic approximation. The valley doses are mainly caused by the scattered photons from the peaks inside the field. We observe that the valley doses increase to

a maximum value and then decreases with the depth. This depth depends on the energy spectrum and in our case the maximum valley dose appeared at a depth of 1.9 cm. The valley PDD also exhibits a higher statistical uncertainty as valley doses are only made of out-of-field doses.

The dose map obtained with penMRT is compared to the dose map obtained by replicating the dose maps obtained by penmain and Gate with one single microbeam (figure 8). There is a good agreement in the peaks doses (less than 1% relative difference), whilst the valley doses differ from 0.5 to 7.5 % between Gate and penMRT, which could be due to the differences in the physics lists that impact the modeling of the transport of low to medium energy photons and electrons.

In order to justify the usage of the source replication model, a MRT dose profile obtained by replication is compared to a MRT dose profile obtained by simulating the multislit collimators (a zoom on the central peak and valley is shown in figure 9).

By using the source replication approach, we have about 0.6% dose under-estimation on valleys, due to the lack of scattering and transmission effects on multislit collimators blades. At the peak center the relative difference is negligible. A 5-10% relative difference is observed in high-gradient areas, i.e. in the microbeam penumbras over 15 μm . This is inherent to the source definition strategy. This validates the source replication approach, neglecting the collimator transmission and scatter effects.

Multi-scale dose maps in unidirectional and multidirectional MRT irradiations. Before testing penMRT in complex treatment conditions, penMRT has been validated against penmain for multi-directional irradiations.

The comparisons between penmain and penMRT for multiple incidences irradiations are represented on figure 10. As the Q-Q test has returned a dose comparisons distributions map that follows the $y=x$ line, it clearly shows the similarity of the two dose distributions. We thus validated penMRT against penmain for microbeam arrays for multiple incidences.

At the end, all implemented features in penMRT were tested by simulating unidirectional, bidirectional and multidirectional treatments. Figure 11 shows the multiscale dose maps alongside with a zoom on the high resolution calculation grid. Simulating each beam requires less than 24 hours on the ESRF cluster. In multidirectional treatment, all the treatment beams can be simulated at the same time. Showing micrometric information on centimetric scale, induces some display artifacts which are visible in the subplots of figure 11. The dose values are however available as shown on the zoomed figure, where display artifacts are no longer seen.

The interpretation of high resolution dose maps can be helped by the analysis of high resolution DVHs. An example of high resolution DVHs obtained on a virtual $1 \times 1 \times 1 \text{ cm}^3$ target centered on the treatment isocenter is also shown on Figure 11. The dose was prescribed such that the whole ROI received a minimum valley dose of 1 Gy in each irradiation beam. The minimum value of DVHs is 1 Gy and 3 Gy, for unidirectional and 3 beams treatments, respectively. The bin width on the DVHs is set at 1 Gy. The peak doses are leading to bell shape plots on the DVHs with the presence of stripes of peak doses as well as hot spots where microbeams cross. To our knowledge these are the first high resolution dose maps and DVHs obtained for MRT treatments using cross-fired beams.

In unidirectional treatments (figure 11.a.III), 70% of the target receives valley doses from 1 Gy to 4 Gy, whilst around 9.8% of the volume receives the peak doses ($> 40 \text{ Gy}$) and 2.32% of the volume receives the doses from the average penumbra values (20-40 Gy). Cumulative dose analysis confirms that 100% of the target benefits from the minimum valley dose (1Gy), and around 12.5 % of the volume is exposed to peak doses. In the case of two perpendicular MRT field treatments (results are not shown as they are implicitly represented in 3 beams treatment analysis), about 61.1% of the target receives the sum of the two valley doses (2-8Gy), whilst about 1.28% of the volume receives the sum of 2 peak doses ($> 90 \text{ Gy}$). 16.51% of the volume receives the doses which come from one peak and one valley (around 55 Gy). Cumulative dose analysis shows that 20 to 23 % of the volume is exposed to lethal doses if the latter are equal to at least one peak dose. In the MRT treatment based on three fields (figure 11.b.III), the percentage of the volume receiving the doses from three valleys decreases to about 46%. About 0.1% of volume has the dose of three covering peaks, whilst 0.31% of the volume takes advantage of two covering peaks and about 17% of the volume receives the dose of two valleys

and one peak. Based on cumulative dose analysis 100% of the volume receives at least the three valley doses and at 30 to 35% of the target volume is covered by lethal doses brought by at least one peak.

Discussion

In this paper, penMRT has been first benchmarked against penmain and Gate for broad beam calculations as well as for a single microbeam irradiation and a full microbeam array. This benchmarking was mandatory to test the fact that the modifications performed in the PENELOPE general purpose main program penmain³⁹ to build penMRT were not affecting the accuracy of the Monte Carlo simulations themselves. This has been validated for various values of C1 et C2 from 0.01 to 0.1. The source replication approach and multidirectional treatment have also been validated.

The penMRT performance tests demonstrate the reliability of penMRT to be used for 3D conformal MRT irradiations. In table 2, the peak to valley dose ratios obtained by penMRT are compared to the PVDR available in the literature. The penMRT calculated PVDR values in a square field composed by an array of 51 microbeams, are in good agreement (0 to 8% relative difference) with the study conducted by Martínez-Rovira *et al.* in 2012 with an approach limited to one unidirectional square field irradiation at a normal incidence to the voxelized phantom²². The study from Martínez-Rovira *et al.*²² is based on a complete simulation of the beamline components (from wiggler to phantom), whilst penMRT is based on an approach that aim at optimizing the simulation time without impairing the results such as the source replication and the use of MRT spectra as generated by the Oasys software⁵⁸ developed at the ESRF. It was thus essential to compare the two approaches in similar cases. The PVDR values calculated by penMRT are also compared to the hybrid dose calculation PVDR values given by Donzelli *et al.*³⁷. In this publication a spectrum with an average energy of 105 keV or 110 keV has been used. In our study, the small animals spectrum with an average energy of around 103.8 keV has been used. A relative difference between 0 to 8.5% can be observed between penMRT and hybrid PVDR values. The highest differences (8.5% and 5.7%, for 5 and 10 mm depth, respectively) are observed mostly in the lower depths, which can be explained by differences in the low energy spectrum components between these two studies. The results are also coherent with the experimental study performed by Livingstone *et al.*¹⁰.

This article is protected by copyright. All rights reserved.

It is also shown that taking into account the photon polarization is important for penumbras and out-of-field doses calculations. The polarization effects should not be neglected, in particular when the prescription is performed on valley doses. Our results were in accordance with the study conducted by De Felici *et al.* on the polarization effect²⁹.

The source replication approach used in penMRT accelerates the simulations with the cost of neglecting the transmission, diffusion and reflection through the MSC. In a recent study from Pellicoli *et al.*⁵⁹ the effect of the MSC on peak and valley doses has been investigated. Based on this study, a perfect collimator assumption might cause an under-estimation of the valley doses from 5% to 30% depending on the field size and the energy spectrum. The peak doses might be less affected with an under-estimation of about 0.2%. The experimental valley doses values found experimentally by Pellicoli *et al.* might however, be slightly overestimated due to the irradiation modality used to retrieve valley doses from HD-V2 Gafchromic films, that might have introduced a blurring effect and increased valley doses. Our source replication validation showed that the valley dose under-estimation would be around 0.6%. However, in order to have an improved precision of the collimator contribution, a mother simulation can be run and a phase-space file (PSF) after the MSC be retrieved, but loading and processing a PSF would increase the simulation time considerably⁶⁰, when compared to the source replication approach. As an alternative, simulating the contribution of multislit blades in the form of multiple virtual sources is also under investigation.

In this study, the capability of penMRT to simulate high-resolution and multi-scale and multidirectional dose maps has been validated. To our knowledge these are the first high resolution dose maps obtained on a cross-fired irradiation scheme using synchrotron generated microbeam arrays. The dose maps are used to extract high-resolution DVHs. This is of particular interest for treatment planning in MRT, with dose metrics representing the complexity of the irradiation. So far, the treatment plans in MRT^{8,61} trials are performed using the hybrid algorithm³⁷, which has a limited spatial resolution due to macroscopic rendering of separated peak and valley dose maps¹⁷. PenMRT enables planning and optimization of MRT treatments using high resolution dose metrics when several microbeams arrays are used. Based on a recent hypothesis in MRT, the radiotherapy toxicity and the treatment efficiency is linked to valley and peak doses, respectively^{8,61}. However,

This article is protected by copyright. All rights reserved.

the role of the array of microbeams, the hot spots and their spatial distribution in a multidirectional irradiation is still unknown. A recent study by Cahoon *et al.*⁶² is pointing to the potential role of the bystander effects linked to the over irradiated cells in the beam passage. PenMRT's generated high resolution dose maps and DVHs, showing the distribution at a micrometric scale of areas covered by peaks, valleys and hot spots is undoubtedly a significant added value to the study of the biological outcome of spatially fractionated radiation therapy. The next step of this work is to perform the experimental validation of penMRT using high resolution detectors irradiated in clinical conditions through end to end studies with conformal fields. The use of variance reduction methods (e.g. interaction forcing) on the speed and accuracy of simulations will be also investigated.

Conclusion

We have developed a multi-scale full MC dose calculation engine, penMRT, which allows the user to obtain dose maps at the micrometric scale for photons irradiations. This engine is optimized for microbeam radiotherapy, but it can be used in other treatment modalities, where a micrometric resolution and a large number of scoring dose bins are required. This code has been benchmarked against two general purpose MC codes: penmain (based on PENELOPE) and Gate (based on Geant4). The ability of penMRT to calculate dose maps in multi-scale grids in unidirectional and multidirectional treatments has been validated. As a main result, the first high-resolution dose maps and associated DVHs ever obtained have been produced, which is bringing a significant added value to treatment planning in spatially fractionated radiation therapy.

Acknowledgements

The authors acknowledge financial support from LabEx PRIMES (ANR-11-LABX-0063/ANR- 1-IDEX-0007). The authors also acknowledge the support from the ESRF computing services for the access to the cluster and resources. The authors personally thank Michael Krisch and Paolo Pellicoli for their support, the fruitful discussions and the spectral data that is implemented in penMRT.

Conflict of interest

The authors have no conflicts to disclose.

This article is protected by copyright. All rights reserved.

Data availability statement

The authors confirm that the data supporting the findings of this study are available within the article.

References

1. Chargari C, Magne N, Guy JB, et al. Optimize and refine therapeutic index in radiation therapy: Overview of a century. *Cancer Treatment Reviews*. 2016;45:58-67. doi:10.1016/j.ctrv.2016.03.001
2. Favaudon V, Caplier L, Monceau V, et al. Ultrahigh dose-rate FLASH irradiation increases the differential response between normal and tumor tissue in mice. *Sci Transl Med*. 2014;6(245). doi:10.1126/scitranslmed.3008973
3. Eling L, Bouchet A, Nemoz C, et al. Ultra high dose rate Synchrotron Microbeam Radiation Therapy. Preclinical evidence in view of a clinical transfer. *Radiotherapy and Oncology*. 2019;139:56-61. doi:10.1016/j.radonc.2019.06.030
4. Montay-Gruel P, Corde S, Laissue JA, Bazalova-Carter M. FLASH radiotherapy with photon beams. *Med Phys*. Published online September 14, 2021:mp.15222. doi:10.1002/mp.15222
5. Bouchet A, Lemasson B, Christen T, et al. Synchrotron microbeam radiation therapy induces hypoxia in intracerebral gliosarcoma but not in the normal brain. *Radiotherapy and Oncology*. 2013;108(1):143-148. doi:10.1016/j.radonc.2013.05.013
6. Bouchet A, Serduc R, Laissue JA, Djonov V. Effects of microbeam radiation therapy on normal and tumoral blood vessels. *Physica Medica*. 2015;31(6):634-641. doi:10.1016/j.ejmp.2015.04.014
7. Smyth LML, Day LR, Woodford K, Rogers PAW, Crosbie JC, Senthil S. Identifying optimal clinical scenarios for synchrotron microbeam radiation therapy: A treatment planning study. *Physica Medica*. 2019;60:111-119. doi:10.1016/j.ejmp.2019.03.019
8. Eling L, Bouchet A, Ocadiz A, et al. Unexpected Benefits of Multiport Synchrotron Microbeam Radiation Therapy for Brain Tumors. Published online 2021:16.
9. Shinohara K, Kondoh T, Nariyama N, Fujita H, Washio M, Aoki Y. Optimization of X-ray microplanar beam radiation therapy for deep-seated tumors by a simulation study. *Journal of X-Ray Science and Technology*. 2014;22(3):395-406. doi:10.3233/XST-140434

10. Livingstone J, Stevenson AW, Häusermann D, Adam JF. Experimental optimisation of the X-ray energy in microbeam radiation therapy. *Physica Medica*. 2018;45:156-161. doi:10.1016/j.ejmp.2017.12.017
11. Duncan M, Donzelli M, Pellicoli P, et al. First experimental measurement of the effect of cardio-synchronous brain motion on the dose distribution during microbeam radiation therapy. *Medical Physics*. Published online 2020:11.
12. Bräuer-Krisch E, Adam JF, Alagoz E, et al. Medical physics aspects of the synchrotron radiation therapies: Microbeam radiation therapy (MRT) and synchrotron stereotactic radiotherapy (SSRT). *Physica Medica*. 2015;31(6):568-583. doi:10.1016/j.ejmp.2015.04.016
13. Yan W, Khan MK, Wu X, et al. Spatially fractionated radiation therapy: History, present and the future. *Clin Transl Radiat Oncol*. 2019;20:30-38. doi:10.1016/j.ctro.2019.10.0
14. Livingstone J, Stevenson AW, Butler DJ, Häusermann D, Adam JF. Characterization of a synthetic single crystal diamond detector for dosimetry in spatially fractionated synchrotron x-ray fields. *Med Phys*. 2016;43(7):4283. doi:10.1118/1.4953833
15. Bartzsch S, Corde S, Crosbie JC, et al. Technical advances in x-ray microbeam radiation therapy. *Phys Med Biol*. 2020;65(2):02TR01. doi:10.1088/1361-6560/ab5507
16. Donzelli M, Bräuer-Krisch E, Nemoz C, Brochard T, Oelfke U. Conformal image-guided microbeam radiation therapy at the ESRF biomedical beamline ID17. *Med Phys*. 2016;43(6):3157-3167. doi:10.1118/1.4950724
17. Ocadiz A, Livingstone J, Donzelli M, et al. Film dosimetry studies for patient specific quality assurance in microbeam radiation therapy. *Physica Medica: European Journal of Medical Physics*. 2019;65:227-237. doi:10.1016/j.ejmp.2019.09.071
18. Slatkin DN, Spanne P, Dilmanian FA, Sandborg M. Microbeam radiation therapy: Microbeam radiation therapy. *Med Phys*. 1992;19(6):1395-1400. doi:10.1118/1.596771
19. Martínez-Rovira I, Sempau J, Fernández-Varea JM, Bravin A, Prezado Y. Monte Carlo dosimetry for forthcoming clinical trials in x-ray microbeam radiation therapy. *Phys Med Biol*. 2010;55(15):4375-4388. doi:10.1088/0031-9155/55/15/012

20. Martínez-Rovira I, Sempau J, Prezado Y. Development and commissioning of a Monte Carlo photon beam model for the forthcoming clinical trials in microbeam radiation therapy: MC photon beam model for MRT clinical trials. *Med Phys*. 2011;39(1):119-131. doi:10.1118/1.3665768
21. Martínez-Rovira I, Prezado Y. Monte Carlo dose enhancement studies in microbeam radiation therapy. *Medical Physics*. 2011;38(7):4430-4439. doi:10.1118/1.3603189
22. Martínez-Rovira I, Sempau J, Prezado Y. Monte Carlo-based treatment planning system calculation engine for microbeam radiation therapy: MC-based TPS calculation engine for MRT. *Med Phys*. 2012;39(5):2829-2838. doi:10.1118/1.4705351
23. Reynard D, Hugtenburg RP. A Monte Carlo intercomparison of peak-to-valley dose ratios and output factors for microbeam radiation therapy. *Radiation Physics and Chemistry*. 2020;176:108980. doi:10.1016/j.radphyschem.2020.108980
24. Stepanek J, Blattmann H, Laissue JA, Lyubimova N, Di Michiel M, Slatkin DN. Physics study of microbeam radiation therapy with PSI-version of Monte Carlo code GEANT as a new computational tool. *Med Phys*. 2000;27(7):1664-1675. doi:10.1118/1.599034
25. Bartzsch S, Lerch M, Petasecca M, Bräuer-Krisch E, Oelfke U. Influence of polarization and a source model for dose calculation in MRT: Influence of polarization and source model in MRT. *Med Phys*. 2014;41(4):041703. doi:10.1118/1.4867858
26. Cornelius I, Guatelli S, Fournier P, et al. Benchmarking and validation of a Geant4–SHADOW Monte Carlo simulation for dose calculations in microbeam radiation therapy. *J Synchrotron Rad*. 2014;21(3):518-528. doi:10.1107/S1600577514004640
27. Dipuglia A, Cameron M, Davis JA, et al. Validation of a Monte Carlo simulation for Microbeam Radiation Therapy on the Imaging and Medical Beamline at the Australian Synchrotron. *Sci Rep*. 2019;9(1):17696. doi:10.1038/s41598-019-53991-9
28. Spiga J, Siegbahn EA, Bräuer-Krisch E, Randaccio P, Bravin A. The GEANT4 toolkit for microdosimetry calculations: Application to microbeam radiation therapy (MRT): Microbeam radiation therapy dosimetry with GEANT4. *Med Phys*. 2007;34(11):4322-4330. doi:10.1118/1.2794170

29. De Felici M, Felici R, del Rio MS, Ferrero C, Bacarian T, Dilmanian FA. Dose distribution from x-ray microbeam arrays applied to radiation therapy: An EGS4 Monte Carlo study: X-ray microbeam dose deposition: An EGS4 study. *Med Phys*. 2005;32(8):2455-2463. doi:10.1118/1.1951043
30. De Felici M, Felici R, Ferrero C, Bravin A, Tartari A, Gambaccini M. Monte Carlo assessment of peak-to-valley dose ratio for MRT. *Nuclear Instruments and Methods in Physics Research Section A: Accelerators, Spectrometers, Detectors and Associated Equipment*. 2007;580(1):489-492. doi:10.1016/j.nima.2007.05.146
31. Orion I, Rosenfeld AB, Dilmanian FA, Telang F, Ren B, Namito Y. Monte Carlo simulation of dose distributions from a synchrotron-produced microplanar beam array using the EGS4 code system 4. *Phys Med Biol*. 2000;45(9):2497-2508. doi:10.1088/0031-9155/45/9/304
32. Hugtenburg RP, Adegunloye AS, Bradley DA. X-ray microbeam radiation therapy calculations, including polarisation effects, with the Monte Carlo code EGS5. *Nuclear Instruments and Methods in Physics Research Section A: Accelerators, Spectrometers, Detectors and Associated Equipment*. 2010;619(1-3):221-224. doi:10.1016/j.nima.2010.01.018
33. Hanson AL, Slatkin DN, Laissue JA. Unidirectional x-ray microbeam radiosurgery of infantile neuraxial malignancies: estimations of tolerable valley doses. In: Kollias N, Choi B, Zeng H, et al., eds. ; 2013:85655G. doi:10.1117/12.2004194
34. Felici MD, Siegbahn EA, Spiga J, et al. Monte Carlo code comparison of dose delivery prediction for microbeam radiation therapy. *J Phys: Conf Ser*. 2008;102:012005. doi:10.1088/1742-6596/102/1/012005
35. Debus C, Oelfke U, Bartzsch S. A point kernel algorithm for microbeam radiation therapy. *Phys Med Biol*. 2017;62(21):8341-8359. doi:10.1088/1361-6560/aa8d63
36. Poole CM, Day LRJ, Rogers PAW, Crosbie JC. Synchrotron microbeam radiotherapy in a commercially available treatment planning system. *Biomed Phys Eng Express*. 2017;3(2):025001. doi:10.1088/2057-1976/aa5f1a

37. Donzelli M, Bräuer-Krisch E, Oelfke U, Wilkens JJ, Bartzsch S. Hybrid dose calculation: a dose calculation algorithm for microbeam radiation therapy. *Phys Med Biol.* 2018;63(4):045013. doi:10.1088/1361-6560/aaa705
38. Day, L. R. J., Donzelli, M., Pelliccioli, P., Smyth, L. M. L., Barnes, M., Bartzsch, S., & Crosbie, J. C. (2021). A commercial treatment planning system with a hybrid dose calculation algorithm for synchrotron radiotherapy trials. *Phys. Med. Biol.*, 15.
39. Salvat F, Fernandez-Varea J M and Sempau J. *PENELOPE-2018, A Code System for Monte Carlo Simulation of Electron and Photon Transport* (Issy-les-Moulineaux: OECD Nuclear Energy Agency);2019 .
40. Rogers DWO. Fifty years of Monte Carlo simulations for medical physics. *Phys Med Biol.* 2006;51(13):R287-R301. doi:10.1088/0031-9155/51/13/R17
41. Sempau J, Badal A, Brualla L. A PENELOPE -based system for the automated Monte Carlo simulation of clinacs and voxelized geometries-application to far-from-axis fields: Automated MC simulation of clinacs with PENELOPE. *Med Phys.* 2011;38(11):5887-5895. doi:10.1118/1.3643029
42. Benmakhlouf H, Bouchard H, Fransson A, Andreo P. Backscatter factors and mass energy-absorption coefficient ratios for diagnostic radiology dosimetry. :27.
43. Bartzsch S, Oelfke U. A new concept of pencil beam dose calculation for 40-200 keV photons using analytical dose kernels. *Med Phys.* 2013;40(11):111714. doi:10.1118/1.4824150
44. Wang XJ, Miguel B, Seuntjens J, Fernández-Varea JM. On the relativistic impulse approximation for the calculation of Compton scattering cross sections and photon interaction coefficients used in kV dosimetry. *Phys Med Biol.* 2020;65(12):125010. doi:10.1088/1361-6560/ab8108
45. Moskvina V, Timmerman R, DesRosiers C, et al. Monte Carlo simulation of the Leksell Gamma Knife®: II. Effects of heterogeneous versus homogeneous media for stereotactic radiosurgery. *Phys Med Biol.* 2004;49(21):4879-4895. doi:10.1088/0031-9155/49/21/003
46. Sempau J, Andreo P. Configuration of the electron transport algorithm of PENELOPE to simulate ion chambers. *Phys Med Biol.* 2006;51(14):3533-3548. doi:10.1088/0031-9155/51/14/017

47. Bernal MA, Liendo JA. An investigation on the capabilities of the PENELOPE MC code in nanodosimetry: PENELOPE code in nanodosimetry. *Med Phys*. 2009;36(2):620-625. doi:10.1118/1.3056457
48. Stewart RD, Wilson WE, McDonald JC, Strom DJ. Microdosimetric properties of ionizing electrons in water: a test of the PENELOPE code system. *Phys Med Biol*. 2002;47(1):79-88. doi:10.1088/0031-9155/47/1/306
49. Bueno G, Déniz O, Carrascosa CB, Delgado JM, Brualla L. Fast Monte Carlo simulation on a voxelized human phantom deformed to a patient: Fast MC simulation on a deformed human phantom. *Med Phys*. 2009;36(11):5162-5174. doi:10.1118/1.3245877
50. Bräuer-Krisch E, Requardt H, Brochard T, et al. New technology enables high precision multislit collimators for microbeam radiation therapy. *Review of Scientific Instruments*. 2009;80(7):074301. doi:10.1063/1.3170035
51. Cruise RB, Sheppard RW, Moskvina VP. PARALLELIZATION OF THE PENELOPE MONTE CARLO PARTICLE TRANSPORT SIMULATION PACKAGE. Published online 2003:11.
52. Bräuer-Krisch E, Serduc R, Siegbahn EA, et al. Effects of pulsed, spatially fractionated, microscopic synchrotron X-ray beams on normal and tumoral brain tissue. *Mutation Research/Reviews in Mutation Research*. 2010;704(1-3):160-166. doi:10.1016/j.mrrev.2009.12.003
53. Sarrut D, Bardiès M, Boussion N, et al. A review of the use and potential of the GATE Monte Carlo simulation code for radiation therapy and dosimetry applications: GATE for dosimetry. *Med Phys*. 2014;41(6Part1):064301. doi:10.1118/1.4871617
54. Depuydt T, Van Esch A, Huyskens DP. A quantitative evaluation of IMRT dose distributions: refinement and clinical assessment of the gamma evaluation. *Radiotherapy and Oncology*. 2002;62(3):309-319. doi:10.1016/S0167-8140(01)00497-2
55. Requardt H, Bravin A, Prezado Y, et al. The Clinical Trials Program at the ESRF Biomedical Beamline ID17: Status and Remaining Steps. In: ; 2010:161-164. doi:10.1063/1.3463164
56. <https://www.esrf.fr/Infrastructure/Computing/NICE/Implementation>

57. Cornelius I, Guatelli S, Fournier P, et al. Benchmarking and validation of a Geant4–SHADOW Monte Carlo simulation for dose calculations in microbeam radiation therapy. *J Synchrotron Rad.* 2014;21(3):518-528. doi:10.1107/S1600577514004640
58. <http://ftp.esrf.eu/pub/scisoft/Oasys/readme.html>
59. Pellicoli P, Donzelli M, Davis JA, et al. Study of the X-ray radiation interaction with a multislit collimator for the creation of microbeams in radiation therapy. *J Synchrotron Rad.* 2021;28(2):392-403. doi:10.1107/S1600577520016811
60. Townson RW, Jia X, Tian Z, Graves YJ, Zavgorodni S, Jiang SB. GPU-based Monte Carlo radiotherapy dose calculation using phase-space sources. *Phys Med Biol.* 2013;58(12):4341-4356. doi:10.1088/0031-9155/58/12/4341
61. Coquery N, Adam JF, Nemoz C, et al. Locomotion and eating behavior changes in Yucatan minipigs after unilateral radio-induced ablation of the caudate nucleus. *Sci Rep.* 2019;9(1):17082. doi:10.1038/s41598-019-53518-2
62. Cahoon P, Giacometti V, Casey F, Russell E, McGarry CK, Prise KM, McMahon SJ. Investigating spatial fractionation and radiation induced bystander effects: a mathematical modelling approach. *Phys Med Biol.* 2021 Oct 19. doi: 10.1088/1361-6560/ac3119. Epub ahead of print. PMID: 34666318.

Figure captions:

Figure 1: (a) Block-diagram of penmain released by Salvat et al.³⁹. (b) Block-diagram of penMRT highlighting voxelized geometry processing alongside with quadric geometry and parallelization.

Figure 2: Geometric characteristics of penMRT. (a) A quadric geometry (b) or/and a voxelized geometry can be taken into account. A source replication option is added to penMRT in order to discard the need to model the multislit collimator. A typical synchrotron generated x-ray filtered spectrum, as used in small animals studies, is represented on the left.

Figure 3: Multi-scale dose calculation grid configuration. The green arrow represents the direction of the incident beam. Zone (I), zone (II) and zone (III) represent the high, medium and low resolution regions, respectively. (a) An example of multi-scale dose calculation grid in which the dose information in the beam entrance and after the target is not needed to be rendered at a micrometric resolution. The high resolution calculation grid is confined to the center of the phantom. (b) Same as “a” but with a 45 degrees beam angle. The grid is rotated to remain perpendicular to the beam axis. (c) The dose map obtained in the “b” configuration is rotated to be presented in the same coordinates as the reference orientation. (d) Post-processing operation performed on the dose map shown in “c”; the dose map is resampled to be presented in an orthonormal grid.

Figure 4: Cross validation of dose maps and dose profiles obtained by penmain, Gate and penMRT in a water phantom irradiated by a $2 \times 2 \text{ cm}^2$ broad beam field at a depth of 2 cm. (a) 2%/1mm relative gamma index test where the dose map of penmain as the reference is compared to penMRT ($C1=C2=0.1$). (b) Comparison of horizontal dose profiles, (c) Relative difference between horizontal dose profiles obtained by penMRT, penmain and Gate (reference: penmain with $C1=C2=0.01$, 0.1 and Gate, respectively.) (d) Comparison of vertical and horizontal dose profiles obtained with penMRT, penmain ($C1=C2=0.1$) and Gate. (e) Relative difference between vertical dose profiles obtained by penMRT, penmain and Gate (reference: penmain with $C1=C2=0.01$, 0.1 and Gate, respectively).

Figure 5: Cross validation of dose maps obtained by penmain, Gate and penMRT in a water phantom irradiated by a $50\mu\text{m} \times 2\text{cm}$ single microbeam field. (a) Relative gamma index test of 2%/5 μm where the dose map of penmain as the reference is compared to penMRT ($C1=C2=0.1$). (b) Horizontal profiles obtained

by penMRT, Gate and penmain. (c) Relative difference between penMRT, penmain and Gate (reference: penmain with $C1=C2=0.01, 0.1$ and Gate, respectively).

Figure 6: (a) PDDs in broad beam obtained by penmain and penMRT with $C1$ and $C2$ values of 0.01, 0.05 and 0.1 and Gate. (b) Relative difference between PDD of penMRT/ penmain (reference: penmain with $C1=C2=0.01$ and 0.1) and penMRT/Gate in the broad beam. (c) PDDs in a single microbeam obtained by penmain and penMRT, with $C1$ and $C2$ values of 0.01, 0.05 and 0.1 and Gate, (d) Relative difference between the PDD obtained by penMRT/penmain (reference: penmain with $C1=C2=0.01$ and 0.1) and penMRT/Gate in the single microbeam.

Figure 7: (a) Dose map for a $2 \times 2 \text{ cm}^2$ MRT irradiation field. The position of the horizontal dose profile is shown with a dashed line. (b) Horizontal dose profile at 2 cm of depth. (c) Central peak (d) Central valley PDD.

Figure 8: (a) Comparison of horizontal MRT profiles in a field created by penMRT and the fields created using single microbeam replication in penmain and Gate. (b) A zoom on horizontal profile. (c) The relative difference between penMRT/penmain and penMRT/Gate horizontal profiles.

Figure 9: (a) Comparison of dose profiles (zoom on the central peak and valley) obtained by source replication approach and modeling a multislit collimator in a water phantom irradiated by a $2 \times 2 \text{ cm}^2$ MRT field at a depth of 2 cm (standard deviation of 2 sigma is demonstrated in this figure). (b) Relative difference of dose profiles of simulated by source replication approach and multislit collimators.

Figure 10: Simulation of a multi-directional treatment. (a.I) A cross-fired dose map given by penMRT, (a.II) The penMRT differential dose volume histogram on a region of interest of $1 \times 1 \times 0.1 \text{ cm}^3$. (b.I) A cross-fired dose map given by a penmain. (b.II) The penmain differential dose volume histogram on the same region of interest. (c) Q-Q plot to investigate the similarity between a.II and b.II.

Figure 11: Dose maps in X-Y plan for irradiation fields of $2 \times 2 \text{ cm}^2$, where X is the horizontal direction perpendicular to the microbeam array direction and Y is representing the depth dose plan. The high

resolution grid of 0.005 (X direction) \times 1 (Y-direction) \times 1 (Z-direction) mm^3 covers a $3 \times 6 \times 3 \text{ cm}^3$ zone and the medium resolution dose grid of $1 \times 1 \times 1 \text{ mm}^3$ covers a $18 \times 18 \times 18 \text{ cm}^3$ of the water phantom. The direction of beam propagation is shown with a green arrow. (a.I) The macroscopic vision of the irradiated zone with a single MRT field showing micrometric and millimetric dose calculation grids on the same axis. (a.II) A zoom on a high-resolution region at the center of figure. (a.III) Differential dose-volume histogram (dDVH) of a region of interest (ROI) irradiated by a single MRT field. To have a better visualization, a zoom on higher dose region is given. (b.I) The macroscopic visualization of the irradiated zone by three MRT fields (0° , 35° and 90° incidences). (b.II) A zoom on a ROI with high resolution. The dose hot spots from two and three crossing peaks can be seen here. (b.III) dDVH of a ROI in three irradiation field treatment with a zoom on higher dose area.

Table 1: A summary of the existing dose calculation engines for MRT.

Algorithm name	Developer and year	Calculation method	Advantages	Limitations	Coupled to a TPS
PenEasy	Martínez-Rovira <i>et al.</i> , 2012 ²²	PENELOPE MC code.	The first precise micrometric dose calculation engine for MRT.	-Time consuming, -Limited to unidirectional treatment, -Only for non-conformal fields.	No
Kernel based	Debus <i>et al.</i> , 2017 ³⁵	Pre-calculated kernels for photons and electrons.	Fast calculation.	-Lack of accuracy in valley doses and heterogeneous medium, -Not able to consider the photon polarization.	Yes VIRTUOS
Ray-tracing	Poole <i>et al.</i> , 2017 ³⁶	Pre-calculated PVDRs.	Fast calculation.	Lack of precision.	Yes Eclipse
Hybrid	Donzelli <i>et al.</i> , 2018 ³⁷	Mixed method: -Photons transport from Geant4 MC code, -Electron transport from	-Fast calculation, -Dose calculation in multidirectional treatment,	-Limited to the macroscopic rendering of separated peak and valley doses.	Yes Eclipse ³⁸

kernel based method.

-Taking into account
the conformal beams.

Table 2: Calculated PVDR in a $2 \times 2 \text{ cm}^2$ MRT field as a function of depth compared to measured and calculated values in quasi-similar conditions reported in literature. In order to have comparable standard deviations, PVDRs are given with 2 sigmas.

Depth (mm)	Peak to valley dose ratio (PVDR)				
	Martínez-Rovira <i>et al.</i> ^{20 a}		Livingstone <i>et al.</i> ^{10 b}	Donzelli <i>et al.</i> ^{37 c}	penMRT ^d
	Monte-Carlo	Gafchromic film	MicroDiamond	Hybrid	
5	42±4	38±6	33±2	47	43±5
10	33±3	33±5	28±4	35	33±3
20	28±2	28±4	24±4	28	28±2
40	25±2	22±3	21±2	23	23±2
50	-	-	21±1	23	22±2
100	23±3	19±3	19±1	21	21±3

^a Average energy of spectrum = 100 keV

^b Average energy of spectrum = 95 keV

^c Average energy of spectrum \approx 105 keV

^d Average energy of spectrum = 103.8 keV